The Astrophysical Journal, 616:L175–L178, 2004 December 1

THE ASSOCIATION OF BIG FLARES AND CORONAL MASS EJECTIONS: WHAT IS THE ROLE OF MAGNETIC HELICITY?

A. Nindos[1] and M. D. Andrews[2]

Received 2004 July 15; accepted 2004 October 19; published 2004 November 1

ABSTRACT

Recently, M. D. Andrews found that approximately 40% of M-class flares between 1996 and 1999, classified according to *GOES* X-ray flux, are not associated with coronal mass ejections (CMEs). Using 133 events from his data set for which suitable photospheric magnetograms and coronal images were available, we studied the preflare coronal helicity of the active regions that produced big flares. The coronal magnetic field of 78 active regions was modeled under the "constant α" linear force-free field assumption. We find that in a statistical sense the preflare value of α and coronal helicity of the active regions producing big flares that do not have associated CMEs is smaller than the coronal helicity of those producing CME-associated big flares. A further argument supporting this conclusion is that for the active regions whose coronal magnetic field deviates from the force-free model, the change of the coronal sign of α within an active region is twice as likely to occur when the active region is about to produce a confined flare than a CME-associated flare. Our study indicates that the amount of the stored preflare coronal helicity may determine whether a big flare will be eruptive or confined.

Subject headings: solar-terrestrial relations — Sun: activity — Sun: corona — Sun: coronal mass ejections (CMEs) — Sun: flares — Sun: magnetic fields

1. INTRODUCTION

Several studies on the possible association of coronal mass ejections (CMEs) and X-ray flares (e.g., see the reviews by Kahler 1992 and Harrison 1995) show that brighter flares are more likely to be associated with CMEs. However, intense soft X-ray flares are neither a necessary nor a sufficient condition for the occurrence of CMEs. Furthermore, flares associated with CMEs tend to have longer durations than average flares, but flares of any duration can be associated with CMEs (Harrison 1995). Andrews (2003) considered the complete list of the X- and M-class *GOES* soft X-ray flares observed during the years 1996–1999. He identified possible CME candidates for the 229 flares of his list with good Large Angle and Spectrometric Coronagraph coverage and concluded that 40% of the M-class flares do not have associated CMEs (however, all X-class flares in his list are CME-associated events). The probability of finding a CME candidate did not depend on the flare location, suggesting that the lack of observed CMEs was not an observational selection effect.

In this Letter, we try to understand why some M-class flares do have associated CMEs while other M-class flares do not. Our data set consists of the events studied by Andrews (2003). For such a task, one needs to study in detail the properties of the active regions (ARs) that produce the big flares. Here we compute the coronal magnetic helicity of the corresponding ARs prior to the flare onset. Our study will demonstrate that the coronal magnetic helicity of the ARs plays an important role concerning the relation of big flares to CMEs. In § 2, we present the concept of magnetic helicity. Our analysis and results are given in § 3. We present conclusions in § 4.

2. CORONAL MAGNETIC HELICITY

The magnetic helicity of a field $\boldsymbol{B}$ within a volume V is defined as $H_m = \int_V \boldsymbol{A}\cdot\boldsymbol{B}\,dV$, where $\boldsymbol{A}$ is the magnetic vector potential. It is different from current helicity, $H_{\rm cur}$, which is defined as $H_{\rm cur} = \int_V \boldsymbol{j}\cdot\boldsymbol{B}\,dV$ with $\mu_0\boldsymbol{j} = \boldsymbol{\nabla}\times\boldsymbol{B}$; H_m is a conserved MHD quantity whereas $H_{\rm cur}$ is not. Furthermore, observationally we obtain only a fraction of $H_{\rm cur}$ because only the vertical component of $\boldsymbol{j}$ can be computed. The magnetic helicity is physically meaningful only when $\boldsymbol{B}$ is fully contained inside V. When this condition is not satisfied (for example, in the solar atmosphere), we define a gauge-independent relative magnetic helicity (hereafter referred to as helicity) of $\boldsymbol{B}$ with respect to the helicity of a reference field $\boldsymbol{B}_p$ having the same distribution of vertical magnetic flux on the surface S surrounding V: $H = \int_V \boldsymbol{A}\cdot\boldsymbol{B}\,dV - \int_V \boldsymbol{A}_p\cdot\boldsymbol{B}_p\,dV$. Being a potential field, it is a convenient choice for $\boldsymbol{B}_p$. The quantity $\boldsymbol{A}_p$ is the corresponding vector potential satisfying $\boldsymbol{\nabla}\cdot\boldsymbol{A}_p = 0$ and being horizontal on S. Then the term $\int_V \boldsymbol{A}_p\cdot\boldsymbol{B}_p\,dV$ vanishes (Berger 1988).

In the solar atmosphere, helicity can change either because of the emergence of twisted field lines that cross the photospheric surface (e.g., Leka et al. 1996) or/and by shearing motions on the photosphere. Such motions include differential rotation (e.g., DeVore 2000) and/or transient flows (e.g., Chae 2001; Nindos & Zhang 2002). On the other hand, when a CME occurs, it carries away part of the helicity of its source magnetic field. Démoulin et al. (2002) and Green et al. (2002) developed a method to compute the coronal helicity H_c of ARs. A photospheric magnetogram is used as a boundary condition for linear force-free field magnetic extrapolations ($\boldsymbol{\nabla}\times\boldsymbol{B} = \alpha\boldsymbol{B}$, with α being constant over the AR). The extrapolated field lines are fitted with the AR's coronal loops. The value of α giving the best overall fit between the models and observations is adopted for the computation of the coronal helicity. Then one follows Berger (1985), and after the derived expression is linearized in order to avoid helicity enhancements close to the resonance values, the resulting coronal helicity is

$$H_c = 2\alpha \sum_{n_x=1}^{N_x}\sum_{n_y=1}^{N_y} \frac{|\tilde{B}^2_{n_x,n_y}|}{(k_x^2+k_y^2)^{3/2}}, \qquad (1)$$

where $\tilde{B}_{n_x,n_y}$ is the magnetic field's Fourier amplitude of the

[1] Section of Astrogeophysics, Department of Physics, University of Ioannina, Ioannina GR-45110, Greece; anindos@cc.uoi.gr.
[2] Computational Physics Inc., Naval Research Laboratory, Code 7660, Washington, DC 20375.

TABLE 1
ACTIVE REGIONS AND LINEAR FORCE-FREE FIELD EXTRAPOLATIONS

Extrapolation	Active Regions (Flare-CME)	Active Regions (Flare, No CME)	Total Number
Acceptable	47	31	78
Both signs of α	15	25	40
Uniform α sign, large deviation	10	5	15

(n_x, n_y) harmonic and $k_x = 2\pi n_x/L$, $k_y = 2\pi n_y/L$, with L being the horizontal extension of the computation box used for the force-free field extrapolations (e.g., see Alissandrakis 1981).

3. RESULTS

From the 229 flares studied by Andrews (2003), we select those that originate within $\pm 50°$ from the central meridian. For the interval that starts 1.5 hr prior to the flare start time, we require the availability of at least one Michelson Doppler Imager (MDI) magnetogram and EUV Imaging Telescope (EIT) 195 Å images obtained with cadence higher than 25 minutes. The above selection criteria yield 133 events for further analysis. For each case, we use the MDI magnetogram taken 25 minutes prior to the flare start time as a boundary condition for linear force-free field extrapolations. This is possible when 1 minute cadence MDI magnetograms are available. When they are not available, we create a magnetogram for the time we need, taking into account the solar rotation and interpolating the two magnetograms obtained closest to the desired time. We do not use magnetograms obtained closer to the flare onsets because sometimes impulsive variations of helicity change rate are associated with flares (Moon et al. 2002a, 2002b). Such helicity changes peak within ± 20 minutes of the X-ray flare peak time in all events studied by Moon et al. (2002a, 2002b).

For each event, the extrapolated field lines are fitted with the corresponding AR's EIT coronal loops. We determine the best value of α following basically the procedure developed by Green et al. (2002). Briefly, the technique works as follows: for each loop, we find the lowest mean distance $d_{\rm mean}$ between the loop and the computed field lines resulting from various values of α. The value of α giving the best overall fit between the models and observations ($\alpha_{\rm best}$) is the one that minimizes $\langle d_{\rm mean}\rangle$. The derived $\alpha_{\rm best}$ is considered satisfactory and used in the subsequent analysis if (1) the derived values of α for individual loops should all have the same sign and (2) $\langle d_{\rm mean}\rangle \leq 1.9$ Mm, which is close to the pixel size of the high-resolution EIT images. The above criteria are used because the constant value of α above an AR is a simplification. The values of $\alpha_{\rm best}$ that survive the two criteria are associated with mean deviations that never exceed 30% of the corresponding $\alpha_{\rm best}$. In Table 1, we give the number of ARs that satisfy both conditions, the number of ARs that do not pass the first condition, and the number of ARs that pass the first condition but do not satisfy the second.

In Figure 1, we show the absolute values of $\alpha_{\rm best}$ of the 78 ARs that passed our two conditions as a function of the flare's peak flux. Each error bar denotes the mean deviation to the value of $\alpha_{\rm best}$ over the AR. Also in Figure 1, we give the histograms of $\alpha_{\rm best}$. The average of all values of $\alpha_{\rm best}$ of Figure 1 is 0.028 ± 0.017 Mm^{-1}. This is about a factor of 4 larger than the average photospheric $\alpha_{\rm best}$ derived by Pevtsov et al. (1995), who studied 69 diverse ARs with varying levels of flare activity. The large difference between the two studies is due to selection effects: our sample consists of ARs observed a few minutes before powerful flares. In Figure 2, we give the scatter plots and his-

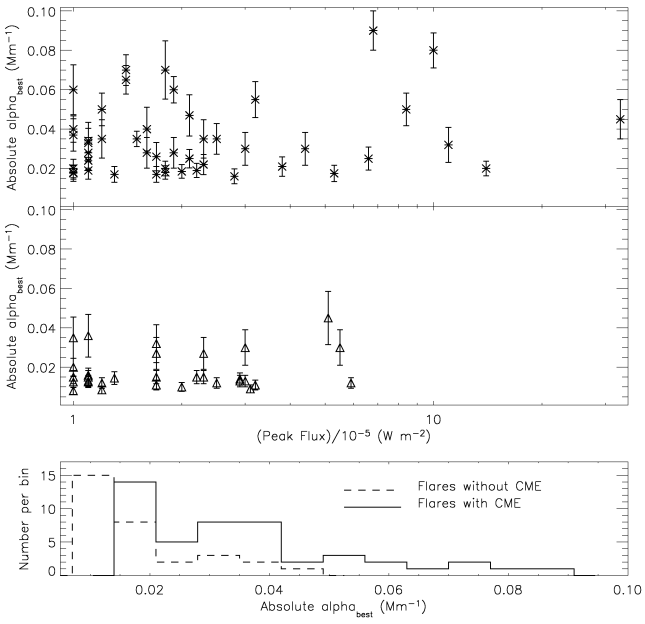

FIG. 1.—*Top*: Scatter plot of the preflare absolute values of $\alpha_{\rm best}$ as a function of the flare's peak X-ray flux for the ARs producing CME-associated flares. *Middle*: Same as the top panel, but for the ARs producing flares that do not have associated CMEs. *Bottom*: Histograms of the values of $\alpha_{\rm best}$ appearing in the top and middle panels. The solid line is the histogram of $\alpha_{\rm best}$ of the ARs that give CME-associated flares, and the dashed line is the histogram of $\alpha_{\rm best}$ of the ARs that produce flares that do not have CMEs.

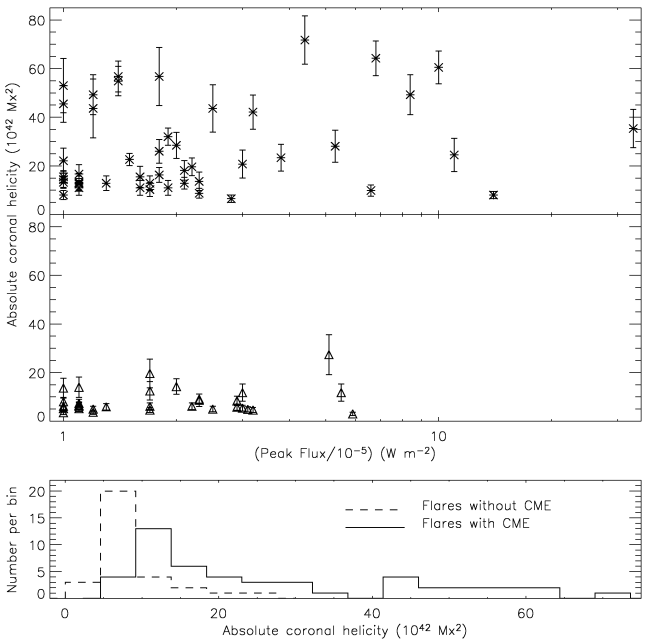

FIG. 2.—Absolute coronal helicity of the 78 ARs appearing in Fig. 1. The format is identical to the format of Fig. 1.

tograms of the absolute coronal helicity, H_c, using the values of $\alpha_{\rm best}$ and equation (1). The average of all values of H_c is $(19.5 \pm 17.0) \times 10^{42}$ Mx^2.

Figures 1 and 2 show that several ARs that give big flares without CMEs have smaller values of $\alpha_{\rm best}$ and H_c than those producing CME-associated flares. This result is statistically significant. We have computed the average $\alpha_{\rm best}$ and H_c separately for the ARs that give flares that do not have CMEs and for the ARs that give CME-associated flares. We find: $\langle \alpha_{\rm no\ cme} \rangle = 0.018 \pm 0.010$ Mm^{-1}, $\langle \alpha_{\rm cme} \rangle = 0.035 \pm 0.018$ Mm^{-1}, and $\langle H_{\rm no\ cme} \rangle = (8.3 \pm 5.2) \times 10^{42}$ Mx^2, $\langle H_{\rm cme} \rangle = (26.8 \pm 18.1) \times 10^{42}$ Mx^2. From the scatter plots, and taking into account the error bars, we find that 45% of the events without CMEs come from ARs with smaller values of $\alpha_{\rm best}$ than the values of $\alpha_{\rm best}$ of each and every AR that gave CME-associated flares. A similar percentage (52%) has been found for the coronal helicities of the ARs without CMEs with respect to the coronal helicities of all ARs producing CME-associated events. The analysis of our results for the $n = 78$ ARs appearing in Figures 1 and 2 shows that the ARs with $\alpha_{\rm best} > 0.02$ Mm^{-1} are a factor of 2.25 more likely to produce flares with CMEs than the ARs with $\alpha_{\rm best} \leq 0.02$ Mm^{-1}. We have used the ϕ coefficient for the evaluation of the statistical significance of the above result. This coefficient is related to χ^2-values through $\chi^2 = n\phi^2$, which can be compared to tabulated χ^2-values with 1 degree of freedom. For our data set, we find $\chi^2 = 16.4$, which means that the null hypothesis (i.e., that there is no association between the initiation of CME-associated flares and whether the AR's $\alpha_{\rm best}$ is bigger or smaller than 0.02 Mm^{-1}) can be rejected at better than the 99.5% confidence level. By the same measures, the ARs with $H_c > 15 \times 10^{42}$ Mx^2 are a factor of 2.4 more likely to produce flares with CMEs than the ARs with $H_c \leq 15 \times 10^{42}$ Mx^2. Here we obtain $\chi^2 = 23.2$, and again the null hypothesis can be rejected at better than the 99.5% confidence level.

The EIT images show low-lying, relatively cool loops. In order to prove that our results are accurate, our best-fit magnetic extrapolations should be checked against *Yohkoh* soft X-ray telescope (SXT) and *Transition Region and Coronal Explorer* (*TRACE*) images. From the 78 ARs, 52 of them have been observed simultaneously by EIT and SXT and seven of them by EIT and *TRACE*. For these ARs, the extrapolated field lines are fitted with the corresponding AR's SXT and *TRACE* coronal loops. In 80% of the cases, the difference between the derived value of $\alpha_{\rm best}$ and the value of $\alpha_{\rm best}$ derived from EIT is less than $\pm 30\%$ of EIT's $\alpha_{\rm best}$. More importantly, the statistical results presented earlier do not change. Furthermore, in one event, vector magnetograms from Huairou Solar Observatory are available, and the $\alpha_{\rm best}$ derived from the vector magnetogram data is also consistent with the corresponding EIT's $\alpha_{\rm best}$.

As an example, in Figure 3 we present preflare EIT, *TRACE* 171 Å, and SXT images of an AR that produced an M8 flare. The coronal images have been obtained on 1998 November 5 18:56, 18:59, and 18:34 UT, respectively. In the top left and the two bottom panels, we overplot selected field lines from the best-fit coronal field models that have been determined from extrapolated field lines that are fitted with the AR's EIT, *TRACE*, and SXT structures. For the extrapolations, we have used an MDI magnetogram obtained at 19:12 UT. In the top right panel, the coronal field lines have been derived from the computation of $\alpha_{\rm best}$ in the photosphere, using Huairou vector magnetogram data (the Huairou data we used were created taking into account solar rotation and interpolating the two vector magnetogram data sets obtained closest to the EIT image). In all cases, the model field lines match the coronal structures relatively well; the most serious deviation appears in the southwestern part of the SXT image as a result of transient activity.

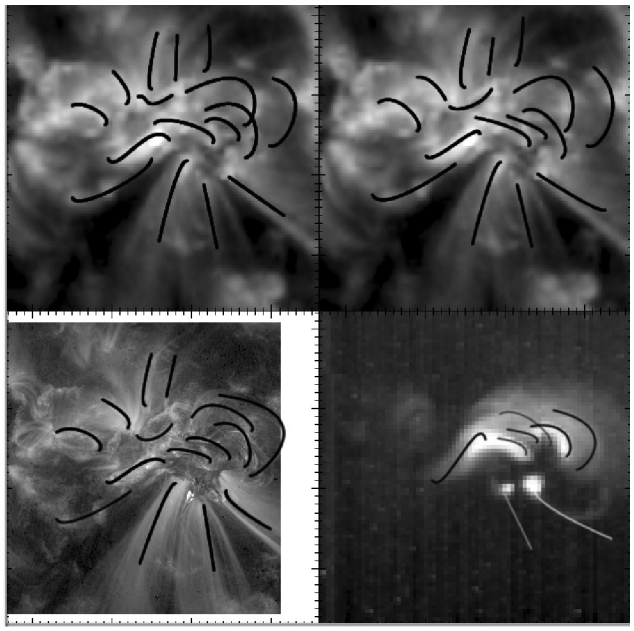

FIG. 3.—Preflare EIT (*top*), *TRACE* (*bottom left*) and *Yohkoh* SXT (*bottom right*) images of NOAA AR 8375. In the top right panel, selected coronal field lines derived from the photospheric $\alpha_{\rm best}$ are presented. In the other panels, the presented field lines result from best-fit extrapolations with respect to the corresponding image's structures. North is up, and west to the right.

The total magnetic flux of the ARs has some correlation with the initiation of CME-associated flares but at a less than statistically significant confidence level: our calculations show that the null hypothesis (i.e., that there is no association between the initiation of CME-associated flares and whether the AR's flux is bigger or smaller than the median value of the magnetic flux of our sample) can be rejected at the 80% confidence level. This result is consistent with the study by Falconer et al. (2002).

Another aspect of our study is that about 40% of our ARs (see Table 1) show coronal structures that cannot be fitted with a uniform value of α over the AR, indicating that the linear force-free approximation cannot represent their coronal magnetic field satisfactorily. Burnette et al. (2004) have argued in favor of the uniformity of the coronal value of α of the ARs they studied. The difference between the two studies may be due to two reasons: (1) part of our coronal data set consists of images with better spatial resolution than the full-frame SXT images they used, and (2) their data set was dominated by mature ARs with relatively simple bipolar topologies and areas either being constant or decreasing. It is also interesting that most ARs whose coronal field deviates from the linear force-free approximation show both signs of α within them (see Table 1). Several such cases become obvious by the appearance of both S-shaped and reversed S-shaped structures in some EIT images. Such structures may correspond to positive and negative signs of α, respectively (e.g., see Rust & Kumar 1996). Furthermore, the change of the coronal sign of α is more frequent in ARs producing flares without CMEs than in those ARs producing CME-associated flares: it happens in 41% of the ARs giving flares without CMEs and only in 21% of the ARs giving CME-associated flares. Kusano et al. (2004) proposed that magnetic reconnection between oppositely sheared loops works as a trigger

mechanism of solar flares. In their calculations, however, it is not clear whether the ejected flux escapes into infinity, accounting for a CME. Their model predicts that the position of flare brightenings should coincide with the magnetic field's shear reversals. The fact that we have used only preflare images makes a direct comparison of our results with their model somewhat difficult.

4. CONCLUSIONS AND SUMMARY

While there is no doubt that CMEs eject helicity from the Sun, their role in the initiation of transient activity is a subject of hot debate. Some argue (e.g., Antiochos & DeVore 1999) that the global helicity by itself yields little information on coronal evolution, while others (e.g., Low 1996) argue that the accumulation of helicity into the corona is at the origin of CMEs. The theoretical work of Amari et al. (2003) supports the idea that a large enough helicity seems to be a necessary condition for an ejection to occur but not a sufficient one. In this Letter, we investigated whether the coronal helicity has anything to do with the fact that some big flares are associated with CMEs while other big flares do not have associated CMEs. Our starting point was the data set of big flares studied by Andrews (2003). From his data set, we selected 133 events for which suitable preflare photospheric magnetograms and coronal images were available. Our computations yielded 78 ARs whose coronal magnetic field could be approximated satisfactorily under the force-free assumption, and subsequently their coronal helicity was computed.

A key conclusion of our study is that the preflare coronal helicity of the ARs producing big flares that do not have CMEs is smaller, in a statistical sense, than the coronal helicity of the ARs producing CME-associated big flares. Overall, our study indicates that the amount of the stored preflare coronal helicity may determine whether a big flare will be a confined event (i.e., a flare without a CME) or an eruptive event (i.e., a CME-associated flare). The findings supporting this conclusion are:

1. The average values of $\alpha_{\rm best}$ and coronal helicity are 0.035 ± 0.018 Mm^{-1} and $(26.8 \pm 18.1) \times 10^{42}$ Mx^2 for the ARs producing eruptive events but only 0.018 ± 0.010 Mm^{-1} and $(8.3 \pm 5.2) \times 10^{42}$ Mx^2 for the ARs producing confined events.
2. About 45%–52% of the ARs producing confined events are associated with values of $\alpha_{\rm best}$ and coronal helicities H_c that are smaller than the values of $\alpha_{\rm best}$ and H_c of all ARs producing eruptive flares.
3. ARs with $\alpha_{\rm best} > 0.02$ Mm^{-1} and $H_c > 15 \times 10^{42}$ Mx^2 are likely to produce confined flares with probabilities of only 29% and 16%, respectively.
4. In the ARs where the linear force-free model is not acceptable, the change of the coronal sign of α within an AR occurs more often in those ARs producing confined flares (in 41% of them) than in the ARs producing eruptive flares (only in 21% of them). This finding may indicate that the distribution of coronal helicity in CME-productive ARs is more coherent than in ARs giving events that do not have associated CMEs.

Finally, a word of caution is needed. Our study does not necessarily imply that the amount of coronal helicity stored in a preflare configuration is the *only* factor that determines whether the flare will be confined or eruptive. A detailed study of the preflare magnetic topology is also required in order to settle this issue. However, such analysis was beyond the scope of this Letter and it will be carried out in the future.

A. N. thanks Professor C. E. Alissandrakis and Dr. S. K. Antiochos for useful discussions. We thank the referee for his/her useful comments, which improved this Letter.

REFERENCES

Alissandrakis, C. E. 1981, A&A, 100, 197
Amari, T., Luciani, J. F., Aly, J. J., Mikic, Z., & Linker, J. 2003, ApJ, 595, 1231
Andrews, M. D. 2003, Sol. Phys., 218, 261
Antiochos, S. K., & DeVore, C. R. 1999, Geophys. Monogr., 111, 187
Berger, M. A. 1985, ApJS, 59, 433
———. 1988, A&A, 201, 355
Burnette, A. B., Canfield, R. C., & Pevtsov, A.A. 2004, ApJ, 606, 565
Chae, J. 2001, ApJ, 560, L95
Démoulin, P., et al. 2002, A&A, 382, 650
DeVore, C. R. 2000, ApJ, 539, 944
Falconer, D. A., Moore, R. L., & Gary, G. A. 2002, ApJ, 569, 1016
Green, L. M., López Fuentes, M. C., Mandrini, C. H., Démoulin, P., van Driel–Gesztelyi, L., & Culhane, J. L. 2002, Sol. Phys., 208, 43
Harrison, R. A. 1995, A&A, 304, 585
Kahler, S. 1992, ARA&A, 30, 113
Kusano, K., Maeshiro, T., Yokoyama, T., & Sakurai, T. 2004, ApJ, 610, 537
Leka, K. D., Canfield, R. C., McClymont, A. N., & van Driel–Gesztelyi, L. 1996, ApJ, 462, 547
Low, B. C. 1996, Sol. Phys., 167, 217
Moon, Y.-J., Chae, J., Wang, H., Choe, G. S., & Park, Y. D. 2002a, ApJ, 580, 528
Moon, Y.-J., et al. 2002b, ApJ, 574, 1066
Nindos, A., & Zhang, H. 2002, ApJ, 573, L133
Pevtsov, A. A., Canfield, R. C., & Metcalf, T. R. 1995, ApJ, 440, L109
Rust, D. M., & Kumar, A. 1996, ApJ, 464, L199